INORGANIC CHEMISTRY FRONTIERS

RESEARCH ARTICLE

View Article Online
View Journal | View Issue

Cite this: *Inorg. Chem. Front.*, 2023, **10**, 5979

$A_{0.5}H_2C_6N_7O_3{\cdot}4H_2O$ (A = Ca^{2+}, Sr^{2+}) iso-cyamelurates with ultra-large π-conjugated group and excellent nonlinear optical properties†

Xiaoguang Du,[a] Fangyan Wang,[b] Fei Liang,*[b] Zhanggui Hu,[a] Yicheng Wu[a,b] and Xinyuan Zhang*[a]

Received 5th July 2023,
Accepted 19th August 2023

DOI: 10.1039/d3qi01251d

rsc.li/frontiers-inorganic

Nonlinear optical (NLO) crystals are the core components of high-performance coherent sources. Their properties can be modulated and improved by molecular design of constituent functional motifs. In this study, inspired by a classical π-conjugated borate group $(B_3O_6)^{3-}$, we discovered a π-conjugated isocyamelurate $[H_2C_6N_7O_3]^-$ anion with colossal π-conjugated orbitals, thus giving ultra-strong anisotropic first-order polarizability and ultralarge second-order susceptibility. Two new alkaline-earth metal isocyamelurates, namely, $Ca_{0.5}H_2C_6N_7O_3{\cdot}4H_2O$ (**I**) and $Sr_{0.5}H_2C_6N_7O_3{\cdot}4H_2O$ (**II**), were successfully synthesized by a facile aqueous solution method. Both **I** and **II** show excellent nonlinear optical properties, including wide band gap (>4.05 eV), large birefringence ($\Delta n \sim 0.24$), and a strong second order harmonic generation response (>5 × KDP). Moreover, **I** and **II** exhibit a broadband ultraviolet photoluminescence around 400 nm, which indicate that they are potential multifunctional optical materials with photon-emission and photon-conversion properties. The first-principles calculations reveal that the $(H_2C_6N_7O_3)^-$ anionic group plays a dominant role in optimizing and enhancing the optical performance of the crystals. This study confirms that there are plenty of opportunities for (iso)-cyamelurates in designing functional crystals with superior properties.

Introduction

Nonlinear optical (NLO) crystals can extend the wavelength of laser to new spectral regions by the use of the second harmonic generation (SHG), DFG, and OPO processes, which are widely used in precision micromanufacturing, laser spectroscopy, optical communication, *etc.*[1–4] The famous anionic group theory has for long time been the research guide in the structural design and screening for high performance NLO materials, and it is of great significance to find high efficiency functional structural units (FBUs), which can simultaneously be provided with large microscopic nonlinear susceptibility and optical anisotropy.[5–10] In this regard, the π-conjugated group is probably the most important and successful group, which promotes the discovery of some commercial crystals, such as $KBe_2BO_3F_2$ (KBBF) with $(BO_3)^{3-}$ group, β-BaB_2O_4 (BBO) with $(B_3O_6)^{3-}$ group, and LiB_3O_5 with $(BO_3)^{3-}$ group.[11–15] Recently, organic FBUs of π-conjugated $(C_3N_3O_3)^{3-}$, structurally similar to inorganic traditional $(B_3O_6)^{3-}$ rings, have been proven to have large nonlinear optical response due to the delocalized p_π electrons and enhanced p_π–p_π interaction.[16–18] Some intriguing crystals with excellent optical properties have been reported, including $KLi(HC_3N_3O_3){\cdot}2H_2O$, $RbLi(HC_3N_3O_3){\cdot}2H_2O$, $K_2Pb(H_2C_3N_3O_3)_4{\cdot}4H_2O$, and $RE_5(C_3N_3O_3)(OH)_{12}$ (RE = Y, Yb, and Lu),[19–22] and these metal cyanurates can exhibit excellent performance with the largest measured SHG responses up to ~5 × KDP and birefringence > 0.18.[23] As a result, this has greatly pushed the development of functional crystals containing π-conjugated groups.

Returning back to anionic group theory, we find that the number of p_π electrons is very important for the conjugacy of a planar group. In order to find more possibilities in conjugated systems, the cyamelurate $(C_6N_7O_3)^{3-}$ group was revisited recently, which has an impressive ultra-large π-conjugated ring with sixteen coplanar atoms. This can be viewed as an extended cyanurate $(C_3N_3O_3)^{3-}$ by inserting a (C_3N_4) motif. As a result, the $(C_6N_7O_3)^{3-}$ anion has a colossal π-conjugated electron configuration of π_{16}^{17} and exhibits strengthened p_π–p_π

[a]*Tianjin Key Laboratory of Functional Crystal Materials, Institute of Functional Crystals, Tianjin University of Technology, Tianjin 300384, China. E-mail: xyzhang@email.tjut.edu.cn*
[b]*State Key Laboratory of Crystal Materials and Institute of Crystal Materials, Shandong University, Jinan 250100, China. E-mail: liangfei@sdu.edu.cn*

†Electronic supplementary information (ESI) available: Additional crystallographic data and experimental and theoretical results, additional tables and figures. CCDC 2277765 and 2277766. For ESI and crystallographic data in CIF or other electronic format see DOI: https://doi.org/10.1039/d3qi01251d

interaction and more delocalized electron distribution than $(C_3N_3O_3)^{3-}$ (π_9^9), thereby leading to a large SHG intensity (>4 × KDP) and birefringence (0.446 @ 1064 nm), as demonstrated in the alkali metal cyamelurate of $K_3C_6N_7O_3{\cdot}2H_2O$.[24] Moreover, iso-cyamelurates have possibilities in the existence of hydroisocyamelurate $(HC_6N_7O_3)^{2-}$ and dihydroisocyamelurate $(H_2C_6N_7O_3)^{-}$, similar to the structural transformation in (iso)cyanurate groups of $(H_xC_3N_3O_3)^{x-3}$ (x = 0, 1, 2), which can also be predicted to have great potential in creating enhanced SHG efficiency and birefringence concurrently by rational design.[25–28] However, to the best of our knowledge, there are a few reports about their related NLO properties and potential applications in this field.

In this study, we explored iso-cyamelurates by introducing alkaline-earth metal cations into a crystal structure with the $[H_2C_6N_7O_3]^{-}$ anion. We successfully synthesized two new iso-cyamelurates, $Ca_{0.5}(H_2C_6N_7O_3)_2{\cdot}4H_2O$ (**I**) and $Sr_{0.5}(H_2C_6N_7O_3)_2{\cdot}4H_2O$ (**II**), which showed excellent nonlinear optical properties. Both of them have strong second-order harmonic generation response (>5 × KDP), wide band gaps (>4.0 eV), and large birefringence ($\Delta n \approx 0.25$ at 1064 nm). Moreover, their structure–property relationship, especially the role of conjugated isocyamelurate group, is elucidated by first-principles calculations.

Experimental section

Reagents

All reagents, melamine ($C_3H_6N_6$, Aladdin, 99%), KOH (Aladdin, ACS), $CaCO_3$ (Aladdin, 99.99%), $SrCO_3$ (Aladdin, AR), Rb_2CO_3 (Aladdin, 99%), were purchased from Shanghai Aladdin Biochemical Technology Co., Ltd and used without further treatment.

Synthesis

Potassium cyamelurate was obtained according to the literature.[29] The potassium cyamelurate (1 mmol, 0.275 g), hydrochloric acid (37%, 2 mL), Rb_2CO_3 (0.5 mmol, 0.116 g), $CaCO_3$ (1 mmol, 0.1 g)/$SrCO_3$ (1 mmol, 0.084 g), and deionized water (40 mL) were mixed and heated to boiling, and then the hot solution was filtered. Transparent crystals were precipitated from the obtained solution when cooled to room temperature (Fig. S1†).

Single crystal X-ray determination

Bruker SMART APEX II 4K CCD single crystal diffractometer was used to collect the single-crystal X-ray diffraction data for **I** and **II** under Mo Kα radiation (λ = 0.71073 Å) at 298 K. Data collection, reduction, and cell refinement were performed by using the software APEX3. The crystal structures were solved by the direct method by intrinsic phasing with the ShelXT structure solution program, and refined using least squares minimization with the ShelXTL refinement package in Olex2.[30,31] Potential missing symmetry of crystal data was checked with the program PLATON30 and no higher symmetry was found.[32] The detailed crystallographic data for $Ca_{0.5}H_2C_6N_7O_3{\cdot}4H_2O$ and $Sr_{0.5}H_2C_6N_7O_3{\cdot}4H_2O$ are listed in Table 1 and Tables S1–S8.†

Powder X-ray diffraction

A Smart Lab 9 kW X-ray diffractometer was used to measure the powder X-ray diffraction with Cu Kα radiation (λ = 1.5418 Å) under room temperature and the 2θ scan range was from 5° to 80° (Fig. S1†).

Thermal analysis

A NETZSCH STA thermal analyzer instrument was used to study the thermogravimetric (TG) analysis and differential scanning calorimetry (DSC) of crystalline samples under the flow of N_2. The powdered compound was placed in Al_2O_3 crucibles ranging from 40 °C to 900 °C.

UV-Vis-NIR diffuse reflectance spectrum

UV-Vis-NIR diffuse reflectance spectrum was measured using a UH4150 UV-Vis-NIR spectrophotometer, and the wavelength range was from 200 nm to 1000 nm. The reflection spectrum was converted to the absorption spectrum according to the Kubelka–Munk function, $F(R) = (1 - R)^2/2R$, where R is the reflectance coefficient.[33,34] The band gap was deduced using a straightforward extrapolation method.[35]

Birefringence measurement

The birefringence was measured using a Nikon Eclipse polarizing microscope E200MV POL under a visible light filter. The calculated birefringence formula was as follows: $\Delta R = \Delta n \times T$, where ΔR, Δn, and T represent the optical path difference, the birefringence, and the thickness of the crystal, respectively.[36,37] Transparent strip crystals were chosen to insure the accuracy. The thickness of the sample was measured by the Bruker Smart Apex II.

Table 1 Crystal data and structure refinements of $Ca_{0.5}H_2C_6N_7O_3{\cdot}4H_2O$ (I) and $Sr_{0.5}H_2C_6N_7O_3{\cdot}4H_2O$ (II)

	I	**II**
Formula weight	312.25	336.02
Crystal system	Orthorhombic	Orthorhombic
Space group	*Fdd*2	*Fdd*2
a (Å)	11.749(7)	11.898(2)
b (Å)	63.01(4)	63.422(9)
c (Å)	5.978(4)	6.0255(10)
V/Å^3	4426(5)	4546.8(13)
Z	16	16
$\rho_{calc.}$ (g cm^{-3})	1.874	1.963
μ (mm^{-1})	0.392	2.477
F(000)	2576.0	2720.0
Flack parameter	0.05(4)	0.07(2)
Reflections collected	22 594	15 400
Final *R* indexes [$I \geq 2\sigma(I)$][a]	R_1 = 0.0519, wR_2 = 0.1007	R_1 = 0.0626, wR_2 = 0.1404
Final *R* indexes [all data][a]	R_1 = 0.1059, wR_2 = 0.1216	R_1 = 0.1140, wR_2 = 0.1635

[a] $R_1 = \sum||F_o| - |F_c||/\sum|F_o|$, $wR_2 = [\sum w(F_o^2 - F_c^2)_2/\sum w(F_o^2)^2]^{1/2}$.

Power SHG measurement

SHG responses of the samples were measured using a Q-switched Nd:YAG laser under 1064 nm wavelength by the Kurtz–Perry technique at room temperature.[38] The crystalline powder was sieved into several different standard sizes: 26–74 μm, 74–100 μm, 100–125 μm, 125–154 μm, 154–180 μm, and 180–200 μm, and KH_2PO_4 (KDP) was used as the reference sample with the same particle size ranges.

Fluorescence measurement

The fluorescence spectra of **I** and **II** were collected using an Edinburgh fluorescence spectrometer at room temperature. A xenon lamp light with a wavelength of 280–310 nm was used as the incident source. The excitation and emission slit functions were set to be 16 and 0.5. The wavelength step is 0.1 nm and the dwell time is 0.02 s. Collection of the spectral lines was repeated twice.

Calculation method

The first-principles calculations for the metal cyamelurates **I** and **II** were performed using the CASTEP package[39] based on density functional theory,[40] which is similar to previous studies on $K_3C_6N_7O_3{\cdot}2H_2O$ and other metal cyanurates.[24,41] An energy cutoff of 900 eV was adopted and a Monkhorst–Pack *k*-point meshes[42] (2 × 2 × 2) in the first Brillouin zone was selected to ensure sufficient accuracy of the calculated results. The exchange–correlation functionals were described by a generalized gradient approximation (GGA) Perdew–Burke–Ernzerhof (PBEsol) functional[43] and the ion–electron interactions for all constituent atoms were modelled by the norm-conserving pseudopotentials.[44] The refractive indices and birefringence values were obtained based on the electronic structures. In the electronic structure calculations, both the lattice constants and atom sites are fully optimized.

Results and discussion

The colorless plate crystals $Ca_{0.5}H_2C_6N_7O_3{\cdot}4H_2O$ (**I**) and $Sr_{0.5}H_2C_6N_7O_3{\cdot}4H_2O$ (**II**) were synthesized by simple evaporation from aqueous solution (Fig. S1†). The measured powder XRD patterns closely matched the diffraction peaks calculated from the crystallographic data, confirming the purity of the sample powder (Fig. S1†). **I** and **II** are isomorphic and both crystallize in the non-centrosymmetric *Fdd*2 space group (no. 43). Herein, only the structure of **I** is taken as an example. As seen in Fig. 1a, the main part of the asymmetric unit of **I** is consisted of a central metal Ca^{2+} coordinated with two O atoms from $(H_2C_6N_7O_3)^-$ anions and six O atoms from six H_2O molecules, and the two $(H_2C_6N_7O_3)^-$ anion planes are in the angle of 61.45°. The coordinated Ca^{2+} cations are aligned along the *a*-axis and the nearest distance of $(H_2C_6N_7O_3)^-$ layers is 3.086 Å (Fig. 1b). In the crystal packing diagram, the isolated asymmetric unit is further interconnected by hydrogen bonds to build a 3D structure (Fig. 1c) with symmetry operator of glide plane (*n*), and crystal water molecules arranged between

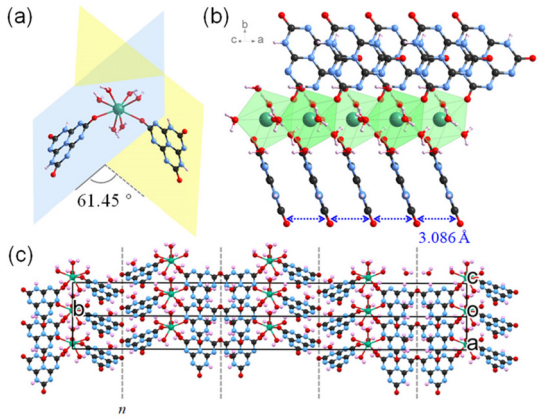

Fig. 1 Crystal structure of $Ca_{0.5}H_2C_6N_7O_3{\cdot}4H_2O$ (**I**). (a) The coordination environment of Ca^{2+}; (b) the arrangement of $(H_2C_6N_7O_3)^-$ anions; (c) the packing diagram of **I** viewed along the [101] direction. Green, red, blue, black, and pink balls represent Ca, O, N, C, and H atoms, respectively.

the layers. As for $Sr_{0.5}H_2C_6N_7O_3{\cdot}4H_2O$ (**II**), the two $(H_2C_6N_7O_3)^-$ anion planes are in the angle of 61.68° in the main part of the asymmetric unit, and the nearest distance between the anion planes is 3.106 Å, which are very similar to **I** (Fig. S2†) but different in the content of water of crystallization in the unit cell reported for $Sr[H_2C_6N_7O_3]_2{\cdot}4H_2O$.[25]

The thermogravimetric (TG) and differential scanning calorimetry (DSC) curves show the weight loss process of **I** and **II**. As seen in Fig. S3,† there are two steps for **I** in the range of 110–900 °C in nitrogen atmosphere. The first weight loss is from 110 to 205 °C corresponding to 4 molecules of H_2O (exp. 23.22%/cal. 23.08%) and the continuous mass loss starts at 205 °C, indicating thermal decomposition of the sample. **II** also displays similar steps of weight loss in the range of 110–900 °C. Such a weight loss process is similar to $LnC_6N_7O_3{\cdot}7H_2O$ (Ln = La, Ce, Pr, Sm, Eu, Gd, Tb, Dy, and Tm) which have been reported previously.[45]

Fig. 2 shows the UV-Vis-NIR diffuse reflection spectra of **I** and **II**. Both **I** and **II** have rather wide band gaps (E_g) of 4.05 eV and 4.07 eV, respectively, corresponding to the cutoff edge of 306 nm and 304 nm. As expected, with the introduction of alkaline-earth metal cations, the obvious enhancement of E_g is realized by comparison with the previously reported alkali

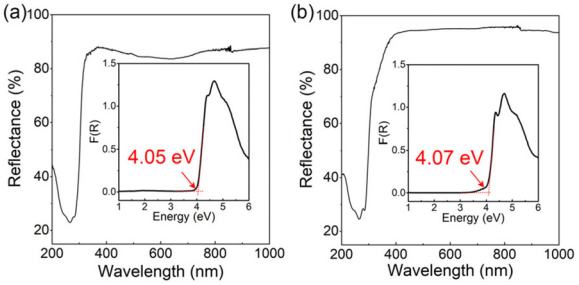

Fig. 2 The UV-Vis-NIR diffuse reflectance spectra of (a) **I** and (b) **II**.

metal cyamelurate $K_3C_6N_7O_3{\cdot}2H_2O$ (2.9 eV). The band gaps of **I** and **II** are comparable or larger than some other compounds featuring π-conjugated FBUs, such as $K_2Pb(H_2C_3N_3O_3)_4{\cdot}4H_2O$ (3.9 eV), $NH_4Sb_2(C_2O_4)F_5$ (3.85 eV), $Na_3C_6N_9{\cdot}3H_2O$ (4.16 eV), $KC_9H_5O_6(H_2O)$ (3.91 eV), and $[C(NH_2)_2NHNO_2][C(NH_2)_3](NO_3)_2$ (3.58 eV).[21,46–49]

Since **I** and **II** crystallize in the NCS space group of *Fdd*2, their NLO optical properties were investigated by SHG measurements using incident laser irradiation at a wavelength of 1064 nm. As shown in Fig. 3a, the SHG intensities of both **I** and **II** increase with the increase of particle size, and finally **I** and **II** exhibit large SHG response of 5.3 times and 6.5 times of KDP, respectively, with phase matching behaviour. The stronger SHG response in the Sr-analogue is similar to that in $Ca_3(C_3N_3O_3)_2$–$Sr_3(C_3N_3O_3)_2$ solid solutions.[16,17] As far as we know, except alkaline-earth metal isocyanurates, *e.g.* $Sr(HC_3N_3O_3){\cdot}2.5H_2O$ and $Sr(HC_3N_3O_3){\cdot}2H_2O$[50,51] without measured SHG values, the NLO properties under 1064 nm incident light of **I** and **II** as isocyamelurates attributed to the extended $(H_2C_6N_7O_3)^-$ anions are comparable or larger than some those of isocyanurates as $KLi(HC_3N_3O_3){\cdot}2H_2O$ (5.3 × KDP), $LiRb(HC_3N_3O_3){\cdot}2H_2O$ (2.7 × KDP), $NaRb_{0.84}Cs_{0.16}HC_3N_3O_3{\cdot}2H_2O$ (3.0 × KDP), as well as other compounds featured with 6-MR π-conjugated groups, such as $CsAlB_3O_6F$ (2.0 × KDP), $(C_5H_6ON)^+(H_2PO_4)^-$ (3.0 × KDP).[19,20,52,53] In addition, both **I** and **II** exhibit a broadband UV photoluminescence (~400 nm) under the excitation of 290 nm (Fig. 3b and S4†). Especially for **II**, the emission spectrum displays that its full width at half maximum (FWHM) is ~82 nm, which is larger than that of previously reported $K_3(C_6N_7O_3){\cdot}2H_2O$ (FWHM ~ 60 nm).[24] Considering **II** also has strong SHG response and large birefringence, it can be regarded as a potential multi-functional material for photonic fields.

Multi-color source orthogonal polarization microscopy was used to estimate the in-plane birefringence of the extinction of **I** and **II** single crystals, and the results are shown in Fig. S5 and S6.† The observed interference colors are second order pink for **I** and second order green for **II**, respectively. According to the Michal-Levy diagram, the corresponding delay values are 1050 nm and 1350 nm, and the measured crystal thickness is about 4.2 μm and 5.5 μm, respectively.

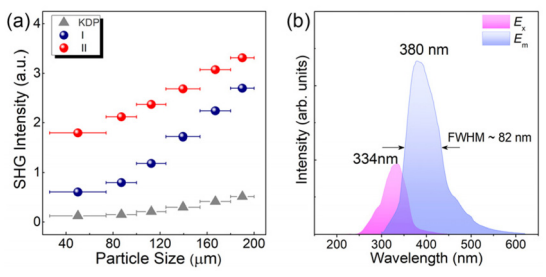

Fig. 3 (a) SHG intensity curves of **I** and **II** and (b) photoluminescent measurement of **II**. Excitation spectrum (E_m = 420 nm) and emission spectrum (E_x = 290 nm).

Thus, the measured birefringence of **I** and **II** is 0.250 and 0.245, respectively. These estimated values are slightly larger than another hydro-isocyamelurate of $Ba(H_2C_6N_7O_3){\cdot}8H_2O$ (0.24 at 550 nm),[27] and show enhancement compared with typical birefringent materials, such as $CaCO_3$ (0.172 at 589 nm) and MgF_2 (0.013 at 253.7 nm).[36,37] Regarding materials with other π-conjugated motifs, *e.g.* β-BBO (0.119 at 546 nm),[13] $Ca_3(BO_3)_2$ (0.097 at 589 nm),[54] and $KLi(HC_3N_3O_3){\cdot}2H_2O$ (0.186 at 514 nm),[19] **I** and **II** maintain a comparable birefringent value, indicating their potential application advantages.

To deeply reveal the origin of the second-order nonlinearity of these two compounds, the electronic structures were calculated. As shown in Fig. S7,† both **I** and **II** are direct gap semiconductors with simulated bandgaps of 3.74 eV and 3.62 eV, respectively, which are close to the experimental values. Fig. 4a and c depict that the Ca^{2+}/Sr^{2+} cations and water molecules show no effect on the electronic states near the forbidden gap, and the main contribution is provided by C 2p, N 2p, and O 2p orbitals from the $(H_2C_6N_7O_3)^-$ anion group. This result conforms to the anionic group theory, which also indicates that the ultra-large conjugated $(H_2C_6N_7O_3)^-$ motif plays a significant role in the optical properties of **I** and **II**.

Furthermore, the optical anisotropy of **I** and **II** was calculated and analyzed. Since **I** and **II** share the same crystal structure and molecular arrangement, they exhibit a large difference in refractive index from the visible to near-IR region with almost the same value. As displayed in Fig. 4b and d, the birefringence n_y–n_x reaches up to 0.24 at 1.06 μm, which is in good agreement with experimental values. For planar $(H_2C_6N_7O_3)^-$ groups, localized C–N/C–O σ-bonds prevail over the in-plane polarizabilities, and delocalized p_π–p_π orbitals around C–N–O rings dominate the out-of-plane polarizabilities, so that the p_π–p_π interaction of iso-cyamelurate groups successfully make

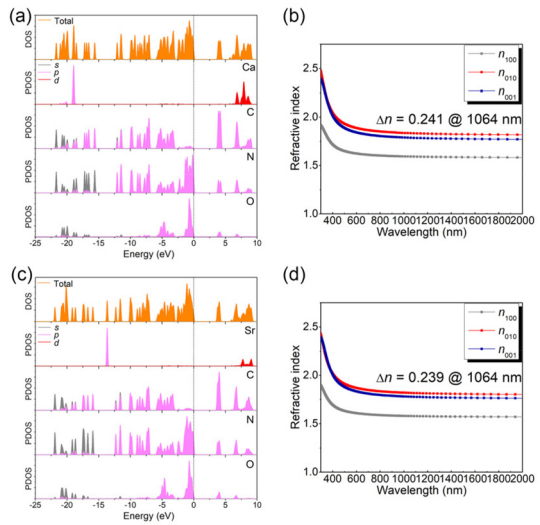

Fig. 4 Total and partial DOS for (a) **I** and (c) **II**; calculated refractive indices for (b) **I** and (d) **II**.

the main contribution to the enhancement of the optical anisotropy.

Conclusions

In summary, two new iso-cyamelurate crystals, namely, $A_{0.5}H_2C_6N_7O_3{\cdot}4H_2O$ (A = Ca^{2+}, Sr^{2+}) containing colossal π-conjugated orbitals were discovered and investigated in detail. They concurrently showed a strong SHG response (5–6.5 × KDP), sufficient birefringence (~0.25 at 1064 nm), wide band gaps (>4.0 eV), and broadband UV photoluminescence, suggesting that they are very promising multi-functional photonic materials. We believe this study would not only be a feasible strategy for designing novel (iso)-cyamelurates with high performance but also enrich new NLO crystals pointing to multi-functional applications.

Conflicts of interest

There are no conflicts to declare.

Acknowledgements

This work is supported by the National Natural Science Foundation of China (Grant No. 52272007, 52002220, 51890864), and the National Key Research and Development Program of China (2021YFA0717800). X. Y. Zhang and F. Liang thank the support from Open Funding of the Key Laboratory of Functional Crystals and Laser Technology, TIPC, CAS.

Notes and references

1 L. L. Cao, H. T. Tian, D. H. Lin, C. S. Lin, F. Xu, Y. L. Han, T. Yan, J. D. Chen, B. X. Li, N. Ye and M. Luo, A flexible functional module to regulate ultraviolet optical nonlinearity for achieving a balance between a second-harmonic generation response and birefringence, *Chem. Sci.*, 2022, **13**, 6990–6997.

2 J. Chen, C. L. Hu, F. Kong and J. G. Mao, High-Performance Second-Harmonic-Generation (SHG) Materials: New Developments and New Strategies, *Acc. Chem. Res.*, 2021, **54**, 2775–2783.

3 L. Lin, X. X. Jiang, C. Wu, L. H. Li, Z. S. Lin, Z. P. Huang, M. G. Humphrey and C. Zhang, $Ba(MoO_2F)_2(XO_3)_2$ (X = Se and Te): First Cases of Noncentrosymmetric Fluorinated Molybdenum Oxide Selenite/Tellurite Through Unary Substitution for Enlarging Band Gaps and Second Harmonic Generation, *ACS Appl. Mater. Interfaces*, 2020, **12**, 49812–49821.

4 W. B. Zhang, J. B. Huang, S. J. Han, Z. H. Yang and S. L. Pan, Enhancement of Birefringence in Borophosphate Pushing Phase-Matching into the Short-Wavelength Region, *J. Am. Chem. Soc.*, 2022, **144**, 9083–9090.

5 K. X. Chen and L. Li, Ordered Structures with Functional Units as a Paradigm of Material Design, *Adv. Mater.*, 2019, **31**, e1901115.

6 G. H. Zou and K. M. Ok, Novel ultraviolet (UV) nonlinear optical (NLO) materials discovered by chemical substitution-oriented design, *Chem. Sci.*, 2020, **11**, 5404–5409.

7 F. J. Hou, D. J. Mei, Y. L. Zhang, F. Liang, J. Wang, J. Lu, Z. S. Lin and Y. D. Wu, $SrZnSnSe_4$: A quaternary selenide with large second harmonic generation and birefringence, *J. Alloys Compd.*, 2022, **904**, 163944.

8 M. J. Ma, J. H. Dang, Y. D. Wu, X. M. Jiang and D. J. Mei, Optimal Design of Mid-Infrared Nonlinear-Optical Crystals: From $SrZnSnSe_4$ to $SrZnSiSe_4$, *Inorg. Chem.*, 2023, **62**, 6549–6553.

9 D. J. Mei, W. Z. Cao, N. Z. Wang, X. X. Jiang, J. Zhao, W. K. Wang, J. H. Dang, S. Y. Zhang, Y. D. Wu, P. H. Rao and Z. S. Lin, Breaking through the "3.0 eV wall" of energy band gap in mid-infrared nonlinear optical rare earth chalcogenides by charge-transfer engineering, *Mater. Horiz.*, 2021, **8**, 2330–2334.

10 W. K. Wang, D. J. Mei, S. G. Wen, J. Wang and Y. D. Wu, Complex coordinated functional groups: A great genes for nonlinear optical materials, *Chem. Phys. Lett.*, 2022, **33**, 2301–2315.

11 C. T. Chen, Y. C. Wu, A. D. Jiang, B. C. Wu, G. M. You, R. K. Li and S. J. Lin, New Nonlinear-Optical Crystal: LiB_3O_5, *J. Opt. Soc. Am. B*, 1989, **6**, 616–621.

12 C. T. Chen, G. L. Wang, X. Y. Wang and Z. Y. Xu, Deep-UV nonlinear optical crystal $KBe_2BO_3F_2$—discovery, growth, optical properties and applications, *Appl. Phys. B*, 2009, **97**, 9–25.

13 C. T. Chen, B. C. Wu, A. D. Jiang and G. M. You, A New-Type Ultraviolet SHG Crystal – Beta-BaB_2O_4, *Sci. China, Ser. B*, 1985, **28**, 235–243.

14 S. X. Guo, X. H. Dong, L. D. Luan, H. M. Zeng, G. H. Zou and Z. E. Lin, Enhanced Second-Harmonic-Generation Response in a KH_2PO_4-Type Calcium Nitrate Carboxylate with Unusual Three-Dimensional Inorganic and Organic Connections, *Inorg. Chem.*, 2022, **61**, 20243–20247.

15 Y. Li, M. Luo, Y. Long, L. Huang, D. J. Gao, G. H. Zou, Z. E. Lin and Y. Zhao, Host-Guest Symmetry and Charge Matching in Glycine-Templated Metal Sulfate-Oxalates Obtained by a Solvent-Free Method, *Inorg. Chem.*, 2023, **62**, 8500–8504.

16 M. Kalmutzki, M. Strobele, F. Wackenhut, A. J. Meixner and H. J. Meyer, Synthesis, structure, and frequency-doubling effect of calcium cyanurate, *Angew. Chem., Int. Ed.*, 2014, **53**, 14260–14263.

17 M. Kalmutzki, M. Strobele, F. Wackenhut, A. J. Meixner and H. J. Meyer, Synthesis and SHG properties of two new cyanurates: $Sr_3(O_3C_3N_3)_2$ (SCY) and $Eu_3(O_3C_3N_3)_2$ (ECY), *Inorg. Chem.*, 2014, **53**, 12540–12545.

18 F. Liang, L. Kang, X. Y. Zhang, M.-H. Lee, Z. S. Lin and Y. C. Wu, Molecular Construction Using $(C_3N_3O_3)^{3-}$ Anions: Analysis and Prospect for Inorganic Metal Cyanurates Nonlinear Optical Materials, *Cryst. Growth Des.*, 2017, **17**, 4015–4020.

19 D. H. Lin, M. Luo, C. S. Lin, F. Xu and N. Ye, KLi($HC_3N_3O_3$)·$2H_2O$: Solvent-drop Grinding Method toward the Hydro-isocyanurate Nonlinear Optical Crystal, *J. Am. Chem. Soc.*, 2019, **141**, 3390–3394.
20 J. Lu, Y. K. Lian, L. Xiong, Q. R. Wu, M. Zhao, K. X. Shi, L. Chen and L. M. Wu, How To Maximize Birefringence and Nonlinearity of π-Conjugated Cyanurates, *J. Am. Chem. Soc.*, 2019, **141**, 16151–16159.
21 Y. Chen, C. L. Hu, Z. Fang and J. G. Mao, $K_2Pb(H_2C_3N_3O_3)_4(H_2O)_4$: a potential UV nonlinear optical material with large birefringence, *Inorg. Chem. Front.*, 2021, **8**, 3547–3555.
22 X. H. Meng, X. Y. Zhang, Q. X. Liu, Z. Y. Zhou, X. X. Jiang, Y. G. Wang, Z. S. Lin and M. J. Xia, Perfectly Encoding π-Conjugated Anions in the $RE_5(C_3N_3O_3)(OH)_{12}$ (RE = Y, Yb, Lu) Family with Strong Second Harmonic Generation Response and Balanced Birefringence, *Angew. Chem., Int. Ed.*, 2023, **62**, e202214848.
23 X. H. Meng, W. L. Yin and M. J. Xia, Cyanurates consisting of intrinsic planar π-conjugated 6-membered rings: An emerging source of optical functional materials, *Coord. Chem. Rev.*, 2021, **439**, 213916.
24 X. Y. Zhang, X. G. Du, J. H. Wang, F. Y. Wang, F. Liang, Z. G. Hu, Z. S. Lin and Y. C. Wu, $K_3C_6N_7O_3·2H_2O$: A Multifunctional Nonlinear Optical Cyamelurate Crystal with Colossal π-Conjugated Orbitals, *ACS Appl. Mater. Interfaces*, 2022, **14**, 53074–53080.
25 N. E. Braml and W. Schnick, New Heptazine Based Materials with a Divalent Cation – $Sr[H_2C_6N_7O_3]_2·4H_2O$ and $Sr[HC_6N_7(NCN)_3]·7H_2O$, *Z. Anorg. Allg. Chem.*, 2013, **639**, 275–279.
26 A. S. Isbjakowa, V. V. Chernyshev, V. A. Tafeenko and L. A. Aslanov, Crystal structures of rare earth cyamelurates obtained under kinetic and thermodynamic controls, *Struct. Chem.*, 2022, **33**, 607–615.
27 Y. Q. Li, W. Q. Huang, Y. Zhou, X. Y. Song, J. Y. Zheng, H. Wang, Y. P. Song, M. J. Li, J. H. Luo and S. G. Zhao, A High-Performance Nonlinear Optical Crystal with a Building Block Containing Expanded π-Delocalization, *Angew. Chem., Int. Ed.*, 2023, **62**, e202215145.
28 Y. Q. Li, X. Zhang, J. Y. Zheng, Y. Zhou, W. Q. Huang, Y. P. Song, H. Wang, X. Y. Song, J. H. Luo and S. G. Zhao, A Hydrogen Bonded Supramolecular Framework Birefringent Crystal, *Angew. Chem., Int. Ed.*, 2023, e202304498.
29 A. Sattler and W. Schnick, Zur Frage der Tautomerie von Cyamelursäure im Kristall, *Z. Anorg. Allg. Chem.*, 2006, **632**, 1518–1523.
30 O. V. Dolomanov, L. J. Bourhis, R. J. Gildea, J. A. K. Howard and H. Puschmann, OLEX2: a complete structure solution, refinement and analysis program, *J. Appl. Crystallogr.*, 2009, **42**, 339–341.
31 G. M. Sheldrick, Crystal structure refinement with SHELXL, *Acta Crystallogr., Sect. C: Struct. Chem.*, 2015, **71**, 3–8.
32 A. L. Spek, Single-crystal structure validation with the program PLATON, *J. Appl. Crystallogr.*, 2003, **36**, 7–13.
33 P. Kubelka and F. Munk, An Article on Optics of Paint Layers, *Z. Tech. Phys.*, 1931, **12**, 593–601.
34 J. Tauc, Absorption edge and internal electric fields in amorphous semiconductors, *Mater. Res. Bull.*, 1970, **5**, 721–729.
35 O. Schevciw and W. B. White, The optical absorption edge of rare earth sesquisulfides and alkaline earth-rare earth sulfides, *Mater. Res. Bull.*, 1983, **18**, 1059–1068.
36 L. L. Cao, G. Peng, W. B. Liao, T. Yan, X. F. Long and N. Ye, A microcrystal method for the measurement of birefringence, *CrystEngComm*, 2020, **22**, 1956–1961.
37 B. E. Sørensen, A revised Michel-Lévy interference colour chart based on first-principles calculations, *Eur. J. Mineral.*, 2013, **25**, 5–10.
38 S. K. Kurtz and T. T. Perry, A Powder Technique for the Evaluation of Nonlinear Optical Materials, *J. Appl. Crystallogr.*, 1968, **39**, 3798–3813.
39 S. J. Clark, M. D. Segall, C. J. Pickard, P. J. Hasnip, M. J. Probert, K. Refson and M. C. Payne, First principles methods using CASTEP, *Z. Kristallogr.*, 2005, **220**, 567–570.
40 W. Kohn, Electronic Structure of Matter, *Rev. Mod. Phys.*, 1999, **71**, 1253–1266.
41 X. Hao, M. Luo, C. S. Lin, G. Peng, T. Yan, D. D. Lin, L. L. Cao, X. F. Long, G. S. Yang and N. Ye, $A(H_3C_3N_3O_3)(NO_3)$ (A = K, Rb): Alkali-Metal Nitrate Isocyanurates with Strong Optical Anisotropy, *Inorg. Chem.*, 2020, **59**, 10361–10367.
42 D. J. Chadi, Special points for Brillouin-zone integrations, *Phys. Rev. B: Solid State*, 1977, **16**, 1746–1747.
43 P. P. John, B. Kieron and E. Matthias, Generalized Gradient Approximation Made Simple, *Phys. Rev. B: Condens. Matter Mater. Phys.*, 1996, **16**, 1746–1747.
44 D. Vanderbilt, Soft self-consistent pseudopotentials in a generalized eigenvalue formalism, *Phys. Rev. B: Condens. Matter Mater. Phys.*, 1990, **41**, 7892–7895.
45 M. Essalhi, M. Mohan, G. Marineau-Plante, A. Schlachter, T. Maris, P. D. Harvey and A. Duong, S-Heptazine N-ligand based luminescent coordination materials: synthesis, structural and luminescent studies of lanthanide-cyamelurate networks, *Dalton Trans.*, 2022, **51**, 15005–15016.
46 B. Jürgens, W. Milius, P. Morys and W. Schnick, Trimerisierung von Dicyanamid-Ionen $C_2N_3^-$ im Festkörper – Synthesen, Kristallstrukturen und Eigenschaften von $NaCs_2(C_2N_3)_3$ und $Na_3C_6N_9·3H_2O$, *Z. Anorg. Allg. Chem.*, 1998, **624**, 91–97.
47 S. F. Li, L. Hu, R. L. Tang, Y. Ma, F. F. Mao, J. Zheng, X. D. Zhang and D. Yan, $KC_9H_5O_6(H_2O)$: A Promising UV Nonlinear-Optical Material with Large Birefringence Based on a π-Conjugated $(C_9H_5O_6)^-$ Group, *Inorg. Chem.*, 2022, **61**, 14880–14886.
48 D. Yan, M. M. Ren, Q. Liu, F. F. Mao, Y. Ma, R. L. Tang, H. Huang, B. Zhang, X. D. Zhang and S. F. Li, $[C(NH_2)_2NHNO_2][C(NH_2)_3](NO_3)_2$: A Mixed Organic Cationic Hybrid Nitrate with an Unprecedented Nonlinear-Optical-Active Unit, *Inorg. Chem.*, 2023, **62**, 4757–4761.
49 D. Zhang, Q. Wang, T. Zheng, L. Huang, L. L. Cao, D. J. Gao, J. Bi and G. H. Zou, $NH_4Sb_2(C_2O_4)F_5$: A novel UV

nonlinear optical material synthesized in deep eutectic solvents, *J. Alloys Compd.*, 2022, **896**, 162921.

50 X. H. Meng, K. J. Kang, F. Liang, J. Tang, W. L. Yin, Z. S. Lin and M. J. Xia, Optimal arrangement of π-conjugated anionic groups in hydro-isocyanurates leads to large optical anisotropy and second-harmonic generation effect, *Inorg. Chem. Front.*, 2020, **7**, 3674–3686.

51 P. Gross and H. A. Höppe, An Expedition on Alkali and Alkaline-Earth Isocyanurate Hydrates: Structure Elucidation, Thermogravimetry, and Spectroscopy, *Z. Anorg. Allg. Chem.*, 2017, **643**, 1692–1703.

52 H. K. Liu, Y. Wang, B. B. Zhang, Z. H. Yang and S. L. Pan, $CsAlB_3O_6F$: a beryllium-free deep-ultraviolet nonlinear optical material with enhanced thermal stability, *Chem. Sci.*, 2019, **11**, 694–698.

53 J. Lu, X. Liu, M. Zhao, X. B. Deng, K. X. Shi, Q. R. Wu, L. Chen and L. M. Wu, Discovery of NLO Semiorganic $(C_5H_6ON)^+(H_2PO_4)^-$: Dipole Moment Modulation and Superior Synergy in Solar-Blind UV Region, *J. Am. Chem. Soc.*, 2021, **143**, 3647–3654.

54 S. Zhang, X. Wu, Y. Song, D. Ni, B. Hu and T. Zhou, Growth of birefringent $Ca_3(BO_3)_2$ crystals by the Czochralski method, *J. Cryst. Growth*, 2003, **252**, 246–250.